From ASA Towards the Full Potential

J. Kollár[1], L. Vitos[1,2], and H.L. Skriver[3]

[1] Research Institute for Solid State Physics,
H-1525 Budapest, P.O.Box 49, Hungary
[2] Condensed Matter Theory Group, Physics Department,
Uppsala University, S-75121 Uppsala, Sweden
[3] Center for Atomic-scale Materials Physics and Department of Physics,
Technical University of Denmark, DK-2800 Lyngby, Denmark

Abstract. To combine the simplicity and efficiency of atomic-sphere approximation (ASA) based electronic structure calculations and the accuracy of full potential techniques, we have developed a *full charge-density* (FCD) method. In this method the charge density is obtained from the output of self-consistent linear muffin-tin orbitals (LMTO) ASA calculations, the Coulomb energy is calculated exactly from the complete, nonspherically symmetric charge density defined within nonoverlapping, space-filling Wigner-Seitz cells, and the exchange-correlation energy is evaluated by means of the local density approximation or the generalized gradient approximation applied to the complete charge-density. The kinetic energy is obtained as the ASA kinetic energy corrected for the nonspherically symmetric charge-density by a gradient expansion. The integration over the Wigner-Seitz cell is carried out by means of the *shape truncation function* technique, which is also discussed in detail. The FCD technique retains most of the simplicity and computational efficiency of the LMTO-ASA method, while several tests for bulk metals and surfaces show that the accuracy of the method is similar to that of full potential methods.

1 Introduction

As a consequence of the rapidly increasing computational facilities followed by the development of computer codes, the *ab initio* electronic structure methods are able to treat more and more complicated problems, closely related to applications, with sufficiently high accuracy. During the last two decades the linear muffin-tin orbitals (LMTO) method [1,2,4,9,3,6,7,5,8] has been one of the most commonly used method in electronic structure calculations. In particular, due to its simplicity and extreme computational efficiency it has been extensively used in total-energy calculations for close-packed high-symmetry systems where the atomic sphere approximation (ASA) may be applied with sufficient accuracy. However, if the local arrangements of atoms deviate strongly from spherical symmetry or the atoms change their positions away from high symmetry positions the ASA cannot be applied. Thus, although the LMTO-ASA may be used to calculate, for instance, the electronic pressure, it cannot in its conventional implementations yield forces and, if uncorrected, the ASA breaks down when used to calculate elastic shear moduli. To increase the number of systems to which the LMTO method may be

H. Dreyssé (Ed.): Workshop 1998, LNP 535, pp. 85–114, 1999.
© Springer-Verlag Berlin Heidelberg 1999

applied, including systems with low symmetry, one has developed a number of full-potential (FP) LMTO techniques [10,11,12,13,14,15]. These techniques are of course highly accurate but lack the efficiency of the LMTO-ASA method. Hence, they may be used in static but not in molecular dynamics calculations and they cannot be used in many applications.

According to the theorem of Hohenberg and Kohn [16], there exists a unique energy functional which is variational in the density. Hence, if the functional is evaluated with a trial density close to the exact ground state density, the error in the total energy is only of second order in the difference between the trial density and the ground state density. This variational property means that in many cases one can achieve the required accuracy simply by evaluating the total energy functional using an appropriate trial density and thus avoiding the most time consuming part of the calculation, the self-consistent iterations. In order to do this, one has to answer the following questions: How does one construct densities which applied in the true functional yield total energies of sufficient accuracy? In the context of the LMTO method one has the related question: How does one evaluate the true functional rather than the approximate ASA functional? It is the purpose of the present paper to provide one answer to these questions.

In the following, we describe and test an efficient technique for total energy calculations based on the LMTO-ASA method in the tight-binding (TB) representation [9,6,7,8]. According to this, we use the complete, non-spherically symmetric charge density generated in self-consistent ASA calculations to evaluate the true energy functional. We have developed the new technique during the last years and used it successfully in many applications [17,18,19], [20,21,22,23,24]. In the first version of the method we used the uncorrected ASA kinetic energy for the total energy calculation and only the electrostatic and exchange-correlation terms of the energy functional were evaluated from a complete non-spherical charge density. In many applications this approximation proved to be sufficiently accurate, like e.g. in studying the ground state atomic volumes of open crystal structures such as the α-phases of the light actinides [19,20,21]. It has turned out, however, that although the ASA kinetic energy is often a suitable approximation, it does not, for instance, yield sufficiently accurate total energies for the small orthorhombic and tetragonal deformations needed in calculations of elastic constants [22]. Therefore we improved the kinetic energy calculation beyond the ASA and thereby take the remaing step towards constructing the true energy functional.

Finally, we point out that although in its present form our *full charge density* (FCD) total energy calculation is based on the conventional LMTO-TB method, it can be an even more promising technique in many applications if it is combined with the recently developed *exact muffin tin orbitals* method by Andersen *et al.* [25]. The new method gives more accurate interstitial charge density and kinetic energy, and thus the accuracy of the FCD total

energy can be substantially improved. The development of such a new FCD technique is in progress.

The structure of the paper is the following: In Section II we set up the FCD total energy and in two subsections we discuss the details of the kinetic and exchange-correlation energy, as well as the Coulomb energy calculations. We put emphasis on the calculation of the kinetic energy correction to the ASA and the technique used in the determination of the intercell Coulomb (Madelung) energy. In Section III we describe the construction of the charge density in a one-center form using a general muffin-tin orbitals formalism. The expressions valid on the LMTO basis are given in the Appendix C. In the calculation of the integrals over the Wigner-Seitz cell we used the *shape truncation function*, or simply *shape function technique*, which is discussed in Section IV. Some important calculational details faced to actual applications are presented and discussed through several examples in Section V. The accuracy of the FCD method is demonstrated in comparison with full potential and experimental results. Finally the paper is ended with the Conclusions.

2 Energy Functional

Within density functional theory the total energy of the system may be decomposed in the form [16]

$$E[n] \equiv G[n] + F[n], \tag{1}$$

where $G[n]$ is a universal functional consisting of the kinetic energy $T[n]$ of the non-interacting system and the exchange-correlation energy $E_{xc}[n]$, i.e.,

$$G[n] \equiv T[n] + E_{xc}[n], \tag{2}$$

and $F[n]$ is the Coulomb contribution to the total energy

$$F[n] \equiv \int v(\mathbf{r}) n(\mathbf{r}) d\mathbf{r} + \frac{1}{2} \int \int \frac{n(\mathbf{r}) n(\mathbf{r}')}{|\mathbf{r} - \mathbf{r}'|} d\mathbf{r} d\mathbf{r}'. \tag{3}$$

Here, $v(\mathbf{r})$ is an external potential. The total charge density $n(\mathbf{r})$ may be given by the sum

$$n(\mathbf{r}) = \sum_R n_R(\mathbf{r}_R) \tag{4}$$

over lattice positions R of atomic-centred charge densities $n_R(\mathbf{r}_R)$ defined within space filling, non-overlapping cells Ω_R, which in turn may be written in the one-centre form [20]

$$n_R(\mathbf{r}_R) = \sum_L n_{RL}(r_R) Y_L(\hat{\mathbf{r}}_R), \tag{5}$$

where L is short-hand notation for (l, m), $\mathbf{r}_R = \mathbf{r} - \mathbf{R}$, and Y_L is a real harmonic. These atomic centred charge densities are normalized within the cells and the total charge density is continuous and continuously differentiable in all space.

In the following we assume that the total energy functional, in accordance with (4) may be partitioned into cell-contributions, i.e. $E[n] = \sum_R E_R[n]$, where $E_R[n] \equiv G_R[n] + F_R[n]$. Due to the non-local character of the interactions these functionals depend on the total density (4). However, in the local density as well as the generalized gradient approximation to the exchange-correlation and kinetic energies G_R depends only on n_R.

2.1 Kinetic and Exchange-Correlation Energy

In the self-consistent ASA based methods both the Schrödinger equation and the Poisson equation are solved within the spherical symmetric approximation for the charge density and the Wigner-Seitz cell. When self-consistency has been reached the Coulomb energy may be evaluated exactly by solving Poisson's equation for the proper charge density and atomic polyhedron. However, the one-electron energies and, hence, the kinetic energy, will reflect the approximation used in the solution of Schrödinger's equation. Therefore, in order to achieve the required accuracy of the total energy we correct the ASA kinetic energy. There are several reasons why a correction to the ASA kinetic energy of the kind presented here has not been previously attempted. First of all, in most LMTO calculations the electrostatic and exchange-correlation terms have been evaluated from a spherically symmetric charge density and, hence, there is no need for a more accurate kinetic energy. Secondly, the kinetic energy, which is obtained from the Kohn–Sham equations [26] as

$$T^{\mathrm{ASA}} = \sum_j^{\mathrm{occ}} \epsilon_j - \int n^{\mathrm{ASA}}(r) v_{\mathrm{eff}}^{\mathrm{ASA}}(r) d\mathbf{r}, \tag{6}$$

where ϵ_j are the one-electron energies, $n(r)$ the electron density, and the $v_{eff}(r)$ the effective potential, is variational in the potential, and it has often been assumed that the ASA kinetic energy is in fact sufficiently accurate. Finally, to improve on the ASA kinetic energy one would need to know an explicit kinetic energy functional, e.g. in the form of a gradient expansion. However, in view of the relatively slow convergence of the known kinetic energy gradient expansions it is not obvious that this would in fact lead to the required accuracy.

The solution to this impasse is to evaluate the main contribution to the kinetic energy in the ASA and then apply an approximate functional form to evaluate the difference between the ASA and the true kinetic energy. This remainder is presumably small and may be obtained with sufficient accuracy by a gradient expansion. A similar approach based on Hartree-Fock densities has been used in atomic calculations by DePristo and Kress [27]. The procedure is closely related to the modern gradient correction to local density functional theory and as we shall demonstrate the corrected FCD method has the accuracy of the full potential methods while retaining most of the simplicity and efficiency of the LMTO-ASA.

In principle, the exchange-correlation energy can be evaluated directly from the total charge density. However, in many cases it is useful to use an expansion arround a uniform or spherical symmetric charge density. Therefore, in the following we consider the universal functional $G[n]$ and we will separate the kinetic and exchange-correlation terms later. The energy density g, corresponding to the functional $G_R[n_R]$, is defined as

$$G_R[n_R] \equiv \int_{\Omega_R} g([n_R], \mathbf{r}_R) d\mathbf{r}_R \tag{7}$$

which may, within the density-gradient approximation, be expressed as [28]

$$\begin{aligned} g([n_R], \mathbf{r}_R) &\equiv t([n_R], \mathbf{r}_R) + \epsilon_{xc}([n_R], \mathbf{r}_R) n_R(\mathbf{r}_R) \\ &= t(n_R, |\nabla n_R|^2, ...) + \epsilon_{xc}(n_R, |\nabla n_R|^2, ...) n_R(\mathbf{r}_R) \\ &\equiv g([n_R]), \end{aligned} \tag{8}$$

where t and $\epsilon_{xc} n$ are the kinetic and exchange-correlation energy densities, respectively. For charge densities which deviate weakly from spherically symmetry $g([n_R])$ may be represented by a Taylor series around the sperically symmetric charge density $n_R^0(r_R) \equiv \frac{1}{\sqrt{4\pi}} n_{R0}(r_R)$, i.e.,

$$\begin{aligned} g([n_R]) = g([n_R^0]) &+ \tilde{n}_R(\mathbf{r}_R) \left. \frac{\partial g([n_R])}{\partial n_R} \right|_{n_R^0} + \nabla \tilde{n}_R(\mathbf{r}_R) \left. \frac{\partial g([n_R])}{\partial \nabla n_R} \right|_{n_R^0} \\ &+ \frac{1}{2} \tilde{n}_R(\mathbf{r}_R)^2 \left. \frac{\partial^2 g([n_R])}{\partial n_R^2} \right|_{n_R^0} + \frac{1}{2} (\nabla \tilde{n}_R(\mathbf{r}_R))^2 \left. \frac{\partial^2 g([n_R])}{\partial (\nabla n_R)^2} \right|_{n_R^0} \\ &+ \tilde{n}_R(\mathbf{r}_R) \nabla \tilde{n}_R(\mathbf{r}_R) \left. \frac{\partial^2 g([n_R])}{\partial n_R \partial \nabla n_R} \right|_{n_R^0} + ... \end{aligned} \tag{9}$$

where $\tilde{n}_R(\mathbf{r}_R) \equiv n_R(\mathbf{r}_R) - n_R^0(r_R)$. As a result, the universal functional may be expanded in the following form

$$G_R[n_R] \; = \; G_R^0[n_R^0] + G_R^1[\tilde{n}_R, n_R^0] + G_R^2[\tilde{n}_R^2, n_R^0] + ..., \tag{10}$$

which may be used to calculate the total energy provided one knows the energy density functions and the corresponding gradients. Unfortunately, this is not the case and one must resort to approximations.

Within modern density functional theory the problem is solved, as far as the exchange-correlation energy $E_{xc;R}[n_R]$ is concerned, by means of the local density approximation (LDA) or generalized gradient approximation (GGA) [29] which yield analytic expressions that may easily be applied in conjunction with the full LMTO charge density. Thus, only the kinetic energy $T_R[n_R]$ remains to be accurately evaluated. Here, the problem is that neither the Kohn–Sham equation (6) in the ASA nor a straight density gradient expansion of the kinetic energy based on the explicit analytic expressions given, for instance, in Ref. [28] have sufficient accuracy when used seperately. However, as we shall show in the following one may by a combination of the two techniques in the form of a density-gradient correction to the ASA obtain kinetic energies with the desired accuracy.

We proceed by isolating the lowest order terms in (7 - 10) which may be evaluated in the ASA and the "small terms" which may be evaluated using a suitable functional form. In the ASA the kinetic energy is obtained from the Kohn–Sham one-electron equations in the form (6) which depends only on the spherical average of the charge density, because the effective one-electron ASA potential is spherically symmetric. Hence, viewed as a functional of an arbitrary density, equation (6) would give the same value for any non-spherically symmetric charge density having the spherical average n_R^0. It may therefore be identified as the kinetic energy belonging to the charge density n_R^0. Thus, we write

$$T_R^0[n_R^0] \approx T_R^{\mathrm{ASA}}[n_R^{\mathrm{ASA}}] + \Delta[n_R^0, n_R^{\mathrm{ASA}}] \tag{11}$$

where T_R^{ASA} is the kinetic energy obtained in the ASA from a spherical symmetric self-consistent calculation and the second term is a "small" shape-correction connected with the fact that the kinetic energy $T_R^0[n_R^0]$ corresponding to the spherically symmetric charge density n_R^0 is defined within the Wigner-Seitz cell at $\mathbf{R}$ while the ASA kinetic energy is defined inside the corresponding atomic sphere. Within the LMTO-ASA method the kinetic energy may be expressed by means of the ASA Hamiltonian H^{ASA} and the one-electron wave functions $\psi_j(\mathbf{r}_R)$ as [30]

$$\begin{aligned} T_R^{\mathrm{ASA}} = & \sum_j^{occ} \int_{S_R} \psi_j{}^*(\mathbf{r}_R)\, H^{\mathrm{ASA}}\, \psi_j(\mathbf{r}_R)\, d\mathbf{r}_R \\ & - \int_{S_R} n_R^{\mathrm{ASA}}(r_R)\, v_{eff}([n_R^{\mathrm{ASA}}], r_R)\, d\mathbf{r}_{\mathbf{R}}, \end{aligned} \tag{12}$$

where $v_{eff}([n_R^{\mathrm{ASA}}], r_R)$ is the effectiv one-electron potential, S_R the atomic Wigner-Seitz radius, and $n_R^{\mathrm{ASA}}(r_R)$ the ASA charge-density normalized wit-

hin the atomic sphere which is equivalent to $n_R^0(r_R)$ inside of the cell and sphere. This form may include the so-called combined correction [7,30]. The shape-correction term in (11) may be obtained as

$$\Delta[n_R^0, n_R^{\mathrm{ASA}}] = \int_{\Omega_R} t([n_R^0])\, d\mathbf{r}_R - \int_{S_R} t([n_R^{\mathrm{ASA}}])\, d\mathbf{r}_R, \tag{13}$$

where the first integral is performed within the Wigner-Seitz cell, Ω_R, and the second one within the atomic sphere.

The shape correction and the kinetic energy part of the higher order terms in (10), i.e., those of first and second order in $\tilde{n}_R$ and $\nabla\tilde{n}_R$, are evaluated by means of a semi-local kinetic energy density functional. In Appendix A we present some functionals used in the actual applications.

For strongly anisotropic electron densities, like in the case of surfaces, the expansion (10) is not convergent. In this case the exchange-correlation energy has to be evaluated by a direct three dimensional integration of the LDA or GGA functional, while the non-spherical kinetic energy correction, i. e. the higher order terms in (10), is calculated as

$$\int_{\Omega_R} t([n_R])\, d\mathbf{r}_R - \int_{\Omega_R} t([n_R^0])\, d\mathbf{r}_R. \tag{14}$$

This procedure is much more time consuming than the Taylor expansion (10).

In order to show the effect of the correction terms to the kinetic energy we consider an orthorhombic shear deformation [22,31] of bcc Mo, which can be used to determine the c_{44} elastic constant. In Fig. 1 we show the total energy, with and without the kinetic energy corrections, versus the relative deformation parameter d.

The energy determined from the experimental shear elastic constant [31] is also shown. We observe that using the ASA kinetic energy the calculated c_{44} is negative and, hence, the bcc structure of Mo will be unstable against such an orthorhombic distortion. Obviously, the ASA kinetic energy is not sufficiently accurate to render the bcc structure of Mo stable. It is only when the kinetic energy correction is applied that a positive c_{44} is obtained which is in fact very close to the measured c_{44} value.

2.2 Coulomb Energy

In this section our aim is to calculate the Coulomb energy of a given charge distribution in a solid with arbitrary symmetry. We devide the total electrostatic contribution belonging to the cell at $\mathbf{R}$ into the intracell, that depends only on the electron density in the cell, and intercell terms, i.e.

$$F_R[n] = F_R^{\mathrm{intra}}[n_R] + F_R^{\mathrm{inter}}[Q]. \tag{15}$$

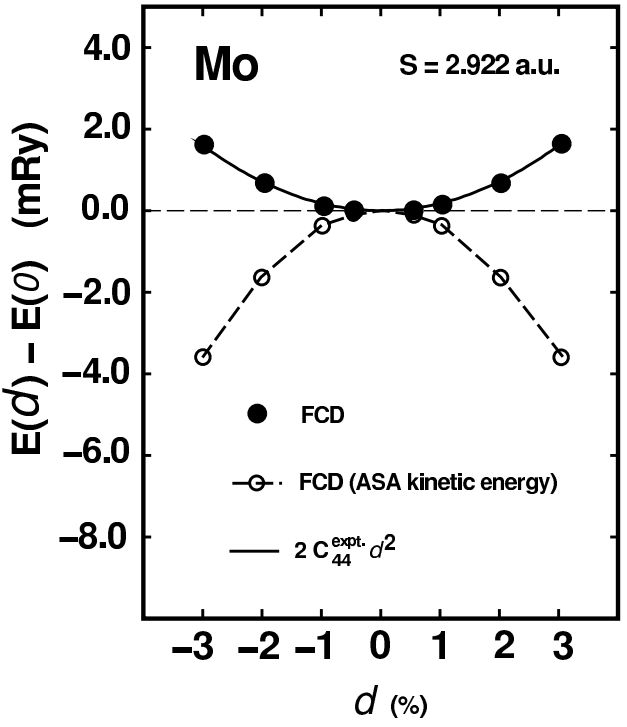

Fig. 1. Change of the total energy of Mo for orthorhombic shear deformation as a function of the relative deformation parameter d.

The intracell energy

$$F_R^{\rm intra}[n_R] \equiv \int_{\Omega_R} \left[-\frac{Z_R}{r_R} + \frac{1}{2} \int_{\Omega_R} \frac{n_R(\mathbf{r}'_R)}{|\mathbf{r}_R - \mathbf{r}'_R|} d\mathbf{r}'_R \right] n_R(\mathbf{r}_R) d\mathbf{r}_R, \qquad (16)$$

where Z_R is the atomic number, may be determined by solving the $l-$dependent Poisson equation or by numerical integration using, for instance, the shape function technique [2,17,32]. Denoting by $\tilde{n}_{RL}(r_R)$ the $Y_L(\hat{\mathbf{r}}_R)$ projection of $n_R(\mathbf{r}_R)$ on a spherical surface of radius r_R that lies inside the cell and performing the angular integrations the expression (16) for the intracell energy can be brought to the form

$$F_R^{\rm intra}[n_R] = \frac{\sqrt{4\pi}}{S} \sum_L \int_0^{S_R^c} \tilde{n}_{RL}(r_R) \left[\left(\frac{r_R}{S} \right)^l P_{RL}(r_R) + \left(\frac{r_R}{S} \right)^{-l-1} Q_{RL}(r_R) \right] r_R^2 dr_R \qquad (17)$$

where

$$P_{RL}(r_R) = \frac{\sqrt{4\pi}}{2l+1} \int_{r_R}^{S_R^c} \tilde{n}_{RL}(r'_R) \left(\frac{r'_R}{S}\right)^{-l-1} (r'_R)^2 dr'_R \tag{18}$$

and

$$Q_{RL}(r_R) = \frac{\sqrt{4\pi}}{2l+1} \int_0^{r_R} \tilde{n}_{RL}(r'_R) \left(\frac{r'_R}{S}\right)^{l} (r'_R)^2 dr'_R - \delta_{L,(0,0)}\, Z_R. \tag{19}$$

Here S_R^c stands for the radius of the sphere circumscribed to the Wigner-Seitz cell Ω_R at $\mathbf{R}$, and S is the average Wigner-Seitz radius. The explicit form for the $\tilde{n}_{RL}(r_R)$ function will be established later using the shape functions.

In Fig. 2 the intracell Hartree energy of fcc Cu is plotted relative to its converged value as a function of $l_{\max}$ used in (17). As may be seen from the figure the energy difference of 0.3 mRy obtained for $l_{\max} = 8 - 11$ is reduced below 0.1 mRy already for $l_{\max} = 12$. In the actual calculations we found that for a wide range of structures a reasonable accuracy of the intracell energy given by (17) can be achieved by performing the summation over l up to $l_{\max} = 8 - 14$.

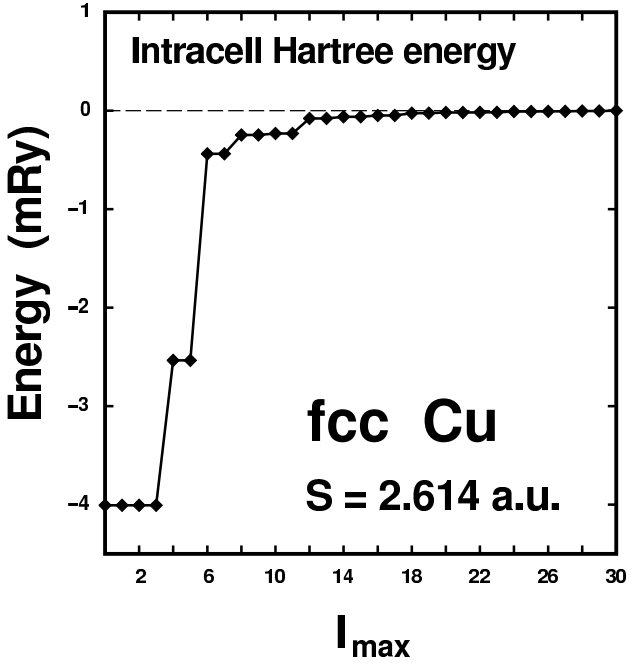

Fig. 2. The convergence test for the intracell Hartree energy of fcc Cu. The results are plotted relative to their converged value as a function of the maximal l value used in (17) or in (43).

The intercell interaction energy belonging to the cell at $\mathbf{R}$ may be written in the following form [17,33]

$$F_R^{\text{inter}}[Q] = -\frac{1}{2S}\sum_{R'L}\frac{1}{2l+1}\left(\frac{b_{RR'}}{S}\right)^l Y_L(\hat{\mathbf{b}}_{RR'})\sum_{L',L''} Q_{RL'}C^L_{L',L''}$$
$$\times\frac{4\pi(2l''-1)!!}{(2l-1)!!(2l'-1)!!}\delta_{l'',l+l'}\sum_{L'''} S_{L'',L'''}(\mathbf{R}'-\mathbf{R}+\mathbf{b}_{RR'})Q_{R'L'''}, \qquad (20)$$

and it can be completely described in terms of the multipole moments defined as

$$Q_{RL} = \frac{\sqrt{4\pi}}{2l+1}\int_{\Omega_R} n_R(\mathbf{r}_R)\, Y_L(\hat{\mathbf{r}}_R)\Big(\frac{r_R}{S}\Big)^l\, d\mathbf{r}_R - \delta_{L,(0,0)}\, Z_R$$
$$= Q_{RL}(S_R^C). \qquad (21)$$

In (20) $S_{L,L'}(\mathbf{R})$ are the conventional LMTO structure constants and $\mathbf{R}'$ runs over the lattice vectors. The *displacement vector* $\mathbf{b}_{RR'}$ has to be chosen in such a way that the circumscribed spheres of the cells in question do not intersect each other (here we assume that the directions of $\mathbf{b}_{RR'}$ and $\mathbf{R}'-\mathbf{R}$ coincide)

$$|\mathbf{R}'-\mathbf{R}| + b_{RR'} > S_R^c + S_{R'}^c. \qquad (22)$$

For the cells with nonoverlapping bounding spheres we can choose $b_{RR'}=0$ so the equation (20) reduces to the well-known form

$$F_R^{\text{inter,no}}[Q] = -\frac{1}{2S}\sum_L Q_{RL}\sum_{\mathbf{R}_{no},L'} S_{L,L'}(\mathbf{R}_{no})Q_{R_{no}L'} \qquad (23)$$

where $\mathbf{R}_{no}$ runs over the cells with nonoverlapping bounding spheres.

For neighbouring cells with overlapping bounding spheres $b_{RR'}$ according to the inequality (22) has to be nonzero. Furthermore, as was pointed out by Gonis *et al.* [33], the outer sum (over l) is conditionally convergent and for a fixed value of the upper limit of the summation over l', l''', it may start to diverge above a certain value of l thus defining a range of convergence of the summation. It was also shown that the range of convergence for the summation in (20) depends sensitively on the choice of $b_{RR'}$ [33]. For larger values of $b_{RR'}$ the sum converges more slowly, but the range of convergence is wider. Therefore we expect an optimal value for $b_{RR'}$ to exist , which is large enough to satisfy (22) and to ensure a wide range of convergence but at the same time the summations over l converge rapidly allowing us to use a reasonably low $l_{\max}$ value in the actual calculations. The choice

$b_{RR'} = |\mathbf{R}' - \mathbf{R}|$ proposed by Gonis *et al.* [33] is suitable for cubic systems [17,18]. However, for a crystal with lower symmetry it may happen that the convergency ranges for different neighbours do not even overlap with this choice of $b_{RR'}$ (e.g. for a tetragonal lattice with large c/a ratio). We have solved this problem by choosing the displacement vector equal to the radius of the circumscribed sphere S_R^c.

On the basis of a simple model [34], described in Appendix B, we have shown that the displacement vector is related to the circumscribed spheres radii as

$$b_{RR'} + |\mathbf{R}' - \mathbf{R}| = (1 + \alpha)(S_R^c + S_{R'}^c), \tag{24}$$

where α is a small positive number which determines the ratio between the maximal orbital quantum numbers included in the outer and inner summations, i. e.

$$l_{\max}/l'_{\max} \simeq \alpha. \tag{25}$$

In order to ensure similar accuracy for different neighbours we have to choose $\alpha = const$. We can see that the limit where α tends to zero corresponds to the lower limit of $b_{RR'} + |\mathbf{R}' - \mathbf{R}|$ in the inequality (22), but in this case the inner summation should go to infinity. For finite $l'_{\max}$, $b_{RR'} + |\mathbf{R}' - \mathbf{R}|$ has to be chosen according to (24) above its lower limit to assure the convergency of the inner summation for any l. With decreasing α, the number of terms in the outer sum decreases. On the other hand, with decreasing α, we need more and more multipole moments in the calculation of the inner sum. By choosing the coordinate system with z axis pointing in the direction of the neighboring atom $\mathbf{R}'$ the summations in (20) can be evaluated efficiently even for very high $l_{\max}$ values. Therefore, it is preferable to choose relatively high α values in order to minimize the computer time needed for the calculation of the multipole moments.

In order to test the accuracy of the intercell energy term evaluated by Eq. (20) and using for the displacement vectors the recipe given in (24) and (25) we calculated the Coulomb energy of a homogeneous charge distribution of several lattices with different symmetry. In these calculations we took $\alpha = 0.5$ and $l_{\max} = 20 - 22$. The scaled Coulomb energies $-E^{\text{Coulomb}}/(Z^2/S)$, i.e., the average Madelung constants are plotted in Fig. 3 as a function of $l_{\max}$ for cubic, tetragonal, $\alpha - Np$ and $\alpha - Pu$ structures. The exact results obtained by the Ewald technique are also indicated in the figure. For the intracell Coulomb energy given in (17) and for the intercell Coulomb energy for cells with nonoverlapping bounding spheres (23) the converged values were used for any $l_{\max}$.

We can see from the figure that the results converge to the exact values smoothly in each case, indicating that using (24) the sums over l converge simultaneously for different neighbouring cells. The relative deviations from the exact values are less than 0.03% for $l_{\max} = 20$ in each case.

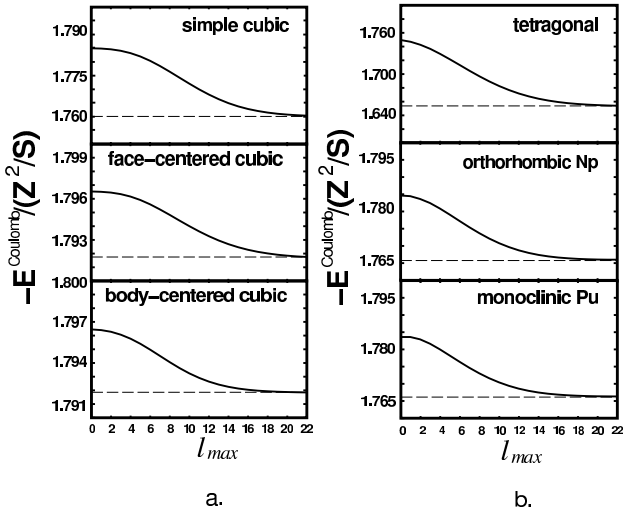

Fig. 3. The scaled average Coulomb energy per cell of a homogeneous charge distribution (Madelung constant) of (**a**) simple, face-centered and body-centered cubic and (**b**) tetragonal, $\alpha - Np$ ($oP8$) and $\alpha - Pu$ ($mP16$) structures as a function of $l_{\max}$. For the tetragonal lattice $c/a = 1.5$ was used. The exact values for the Madelung constants obtained by the Ewald procedure are indicated by dashed lines.

3 Construction of the Charge Density

It was shown by Andersen *et al.* [9,35] that even for open structures such as the diamond structure one may obtain good charge densities by means of an LMTO-ASA potential. In their approach, however, the output charge density is given in a multi-centre form which requires double lattice summations and is therefore less suitable in total energy calculations. Our aim is to rewrite the output ASA charge density in a one-centre form (5). This expression is simple to evaluate and well suited for the integration in the Wigner-Seitz cell at $\mathbf{R}$.

The muffin-tin (MT) orbitals for the low l orbital quantum numbers are defined as [35]

$$\chi_{RL}(\epsilon, \mathbf{r}_R) = Y_L(\hat{\mathbf{r}}_R) \begin{cases} \varphi_{Rl}(\epsilon, r_R) + P_{Rl}(\epsilon) j_l(\kappa, r_R) & \text{for } r_R \leq S_R \\ n_l(\kappa, r_R) & \text{for } r_R > S_R, \end{cases} \quad (26)$$

where $\varphi_{Rl}(\epsilon, r_R)$ is solution of the radial Schrödinger equation, $\kappa^2 \equiv \epsilon - v_0$ is the "kinetic energy in the interstitial region", j_l and n_l are, respectively, regular and irregular solutions at the origin of the radial wave equation for the constant potential v_0 (the muffin-tin zero), and $P_{Rl}(\epsilon)$ is the potential function. In a standard self-consistent calculation only the s, p, d(and f) partial waves are included in the basis set, therefore in (26) $l \leq l_{\max} = 2$(or 3).

The trial wave function for the energy ϵ is set up as the linear combination of the MT orbitals

$$\psi(\epsilon, \mathbf{r}) = \sum_{RL} \chi_{RL}(\epsilon, \mathbf{r}_R) u_{RL}. \tag{27}$$

The expansion coefficients u^j_{RL} as well as the energies ϵ_j are determined from the condition that the wave function $\psi(\epsilon, \mathbf{r})$ should be a solution of the Schrödinger equation for the muffin-tin potential

$$v_R(\mathbf{r}_R) = \begin{cases} v_R(r_R) & \text{if } r_R \leq S_R \\ v_0 & \text{if } r_R > S_R \end{cases}. \tag{28}$$

In order to set up algebraic formulation of this condition we expand the tails of the $n_L(\kappa, \mathbf{r}_R) \equiv n_l(\kappa, r_R) Y_L(\hat{\mathbf{r}}_R)$ envelope functions arround the site $\mathbf{R}'$ in terms of the $j_{L'}(\kappa, \mathbf{r}_{R'}) \equiv j_{l'}(\kappa, r_{R'}) Y_{L'}(\hat{\mathbf{r}}_{R'})$ functions, i.e.

$$n_L(\kappa, \mathbf{r}_R) = -\sum_{L'} j_{L'}(\kappa, \mathbf{r}_{R'})\, S_{R'L',RL}(\kappa). \tag{29}$$

Here the expansion coefficients are the well known structure contants. It is very important to note that for each l the l' summation in (29) goes to infinity, and, because at high orbital quantum numbers the centrifugal potential becomes dominant, all the high l' terms from the right hand side of (29) are solutions of the Schrödinger equation.

For the energies ϵ_j where nontrivial solution of the secular or tail cancellation equation exists the multi-centre form of the wave function (27) inside the MT sphere at $\mathbf{R}'$ reduces to the one-centre form

$$\psi(\epsilon_j, \mathbf{r}_{R'}) \sim \sum_{L'} \varphi_{R'L'}(\epsilon_j, \mathbf{r}_{R'}) u^j_{R'L'} \;\text{ if }\; r_{R'} \leq S_{R'}. \tag{30}$$

This is the expression that is used during the self-consistent iterations. In (30) two significant approximations have been made: i) the use of the incorrect basis functions in the overlap region, and ii) the neglect of the high l' terms in the expansion (29).

In the case of overlapping spheres, there is, in the region of overlap, an uncancelled remainder which is the superposition of the functions

$$f_{RL}(\epsilon, \mathbf{r}_R) \equiv \chi_{RL}(\epsilon, \mathbf{r}_R) - n_L(\kappa, \mathbf{r}_R) = f_{Rl}(\epsilon, r_R) Y_L(\hat{\mathbf{r}}_R) \Theta_R(\mathbf{r}_R) \tag{31}$$

coming from the neighbouring sites [35]. Here,

$$f_{Rl}(\epsilon, r_R) = \varphi_{Rl}(\epsilon, r_R) + P_{Rl}(\epsilon) j_l(\epsilon, r_R) - n_l(\epsilon, r_R), \tag{32}$$

and $\Theta_R(\mathbf{r}_R)$ is a step function, which is 1 inside and zero outside the MT sphere at $\mathbf{R}$. Thus, in the case of overlapping spheres centered at $\mathbf{R}$ the wave function at $\mathbf{R'}$, i.e. $r_{R'} \leq S_{R'}$, should be corrected as [35]

$$\psi(\epsilon_j, \mathbf{r}_{R'}) \sim \sum_{L'} \varphi_{R'L'}(\epsilon_j, \mathbf{r}_{R'}) u^j_{R'L'} + \sum_R \sum_{L'} f_{RL'}(\epsilon_j, \mathbf{r}_R) u^j_{RL'}. \tag{33}$$

In Ref. [20] we describe a method whereby the f function can be included in the one-centre form of the charge density. In many systems we found that this correction is negligible compared to the effect of the high l' terms from the expansion (29). Therefore, here we focus on these terms and present a technique how the high tail components can be taken into account when the one-centre charge density is constructed.

Including the high l' terms in (29) the approximate wave function can be written in the following simple one-centre form

$$\psi(\epsilon_j, \mathbf{r}_{R'}) = \sum_{L'} \varphi_{R'L'}(\epsilon_j, \mathbf{r}_{R'}) u^j_{R'L'} - \sum_{L'}{}' j_{L'}(\kappa_j, \mathbf{r}_{R'}) u^j_{R'L'}, \tag{34}$$

where the second summation includes only terms with $l' > l_{\max}$. This expression is valid inside and outside of the MT spheres as well. When $r_{R'} > S_{R'}$ the partial waves $\varphi_{R'l'}$ has to be substituted by the proper free electron solution $n_{l'} - P_{R'l'} j_{l'}$. In (34) we have extended the definition of the expansion coefficients for the high l' quantum numbers, i.e.,

$$u^j_{R'L'} \equiv \sum_{RL} S_{R'L',RL}(\kappa_j) u^j_{RL} \quad \text{for} \quad l' > l_{\max} \quad \text{and} \quad l < l_{\max}. \tag{35}$$

In this expression the off-diagonal ($l' > l$) structure constants are involved. In the conventional, unscreened, MTO method the calculation of these matrix elements is obvious. In the case of tight-binding representation the high-low subblock of the structure constants is constructed using the so called "blowing-up" technique [7]. The screening parameters for the high l indices are set to zero, and therefore the internal l'' summation in the Dyson equation [7], written for the high-low subblock,

$$S^\alpha_{R'L',RL}(\kappa) = S^0_{R'L',RL}(\kappa) + \sum_{R''L''} S^0_{R'L',R''L''}(\kappa) \alpha_{R''L''} S^\alpha_{R''L'',RL}(\kappa) \tag{36}$$

is truncated at $l''_{\max} = l_{\max}$. Therefore, having the low-low subblock of the screened structure constant and using the high-low unscreened matrix elements, $S^0_{R'L',RL}$ we can determine by simple matrix multiplication the high-low block of the screened structure constants.

The one-centre form of the charge density can be obtained from Eq. (34) and (35). Using a compact notation for the radial functions, i.e.

$$\phi_{Rl}(\epsilon, r_R) = \begin{cases} \varphi_{Rl}(\epsilon, r_R) & \text{if } l \leq l_{\max} \\ -j_l(\kappa, r_R) & \text{if } l > l_{\max}, \end{cases} \tag{37}$$

we obtain the following expression for the partial components of the full charge density

$$n_{RL}(r_R) = \sum_{L''L'} C^L_{L''L'} \sum_j^{occ.} \phi_{Rl''}(\epsilon_j, r_R) u^{j*}_{RL''} u^j_{RL'} \phi_{Rl'}(\epsilon_j, r_R), \tag{38}$$

where $C^L_{L''L'}$ are the real Gaunt numbers. In (38) both l'' and l' summations includes all the terms up to $l'_{max} > l_{max}$. Similar expressions valid for the LMTO basis set are given in Appendix C. In practical applications we found that for an accurate representation of the non-spherical charge density $l'_{\max}$ should be about $8 - 12$ depending on the structure.

When both the overlap correction (33) and the high l' tails (34) are included in the charge density besides the terms from (38) or (64) and those from Ref. [20] one has to include the cross terms, $f_{RL''} j_{L'}$ and $j_{L''} f_{RL'}$ as well.

In Fig. 4 we present charge density contour plots for hexagonal graphite calculated at the theoretical equilibrium volume using Eq. (64) given in Appendix C. From a comparison of the present plots withthose calculated using a full-potential method [36], we can conclude that the effect of the non-spherical potential terms, neglected in the present self-consistent LMTO calculation, have minor effects on the valence charge distribution. The ASA potential describes very well the strongly covalent double humped character of the C-C bonds in the hexagonal graphite. Futher examples of the application of the above technique for the calculation of charge densities are given in Refs. [20, 37].

Finally we note that, because the high l' tails and the shape of the cell are neglected during the self-consistent iterations, the total charge density given by (5) and (38) will not be exactly normalized within the Wigner-Seitz cell. This difficulty can be overcome by a simple spherical symmetric renormalization of the charge density within the cells.

4 Shape Function Technique

In order to calculate the different energy terms discussed earlier, we need a technique to integrate over the W-S cell. To carry out this integration

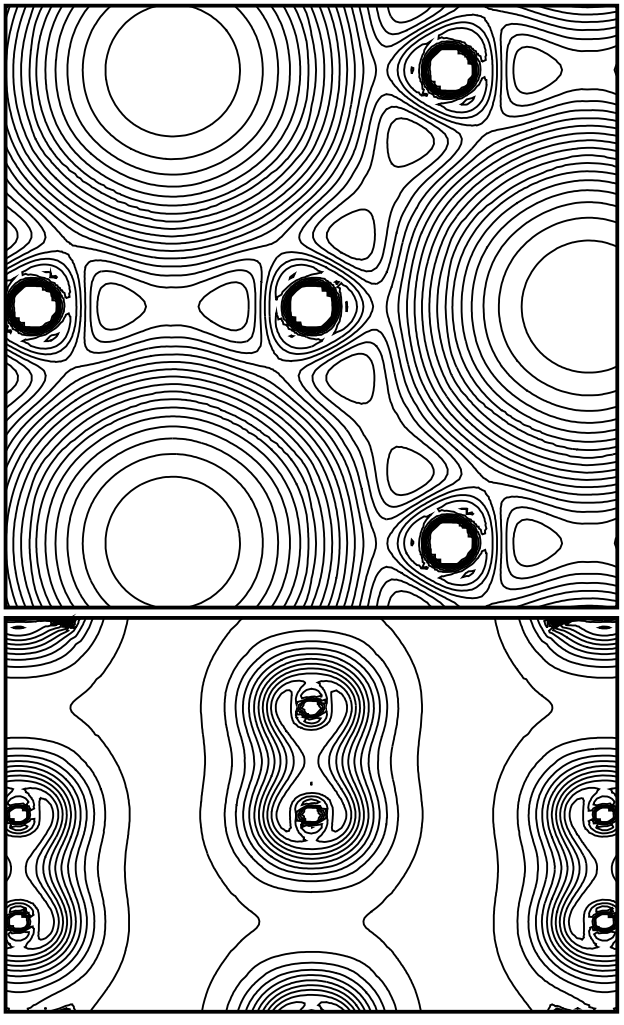

Fig. 4. Charge density contours (in electron/a.u.^{3}) of the *hexagonal* graphite within an atomic layer (left) and in a plane perpendicular to the layers (right). The density was calculated by the TB-LMTO using the one enter form (64).

we use the so-called *shape function technique* [2,17,32] which was recently implemented by Drittler *et al.* [38] in their development of a full-potential Korringa-Kohn-Rostoker multiple scattering method. An alternative scheme to treat interstitial integrals has been proposed by Savrasov and Savrasov [15]. Here, we apply the original version of the method and define the following shape function

$$\sigma_R(\mathbf{r}_R) = \begin{cases} 1 & \text{for } \mathbf{r}_R \in \Omega_R \\ 0 & \text{otherwise} \end{cases} \tag{39}$$

which can be expanded in terms of real harmonics

$$\sigma_R(\mathbf{r}_R) = \sum_L \sigma_{RL}(r_R) Y_L(\hat{\mathbf{r}}_R). \tag{40}$$

Here $\sigma_{RL}(r_R)$ are the partial components of the shape function. By means of the shape function any integral over the W-S cell may be transformed into an integral over the sphere which circumscribes the cell, i.e.

$$\int_{\Omega_R} n_R(\mathbf{r}_R)\ K[n]\ d\mathbf{r}_R = \int_{S_R^c} \sigma_R(\mathbf{r}_R)\ n_R(\mathbf{r}_R)\ K[n]\ d\mathbf{r}_R. \tag{41}$$

Here $K[n]$ can be an arbitrary functional of electron density, for example, the kinetic and exchange-correlation energy density from Eqns. (10,13,14), or the Coulomb potential from Eq. (16), etc. The quantity $\sigma_R(\mathbf{r}_R)\ n_R(\mathbf{r}_R)$ can be expanded in terms of real harmonics

$$\sigma_R(\mathbf{r}_R)\ n_R(\mathbf{r}_R) \equiv \sum_L \tilde{n}_{RL}(r_R) Y_L(\hat{\mathbf{r}}_R), \tag{42}$$

where the partial radial functions represent the $Y_L(\hat{\mathbf{r}}_R)$ projections of the charge density on a spherical surface that lies inside the Wigner-Seitz cell. These functions are used in Section II in the evaluation of the Coulomb energy. In terms of the partial components of the shape function and of the charge density they can be expressed as

$$\tilde{n}_{RL}(r_R) = \sum_{L',L''} C^L_{L',L''} n_{RL'}(r_R) \sigma_{RL''}(r_R), \tag{43}$$

where $C^L_{L',L''}$ are the real Gaunt coefficients.

4.1 Evaluation of the Shape Functions

In order to determine the partial components of the shape function (39)

$$\sigma_{RL}(r_R) = \int \sigma_R(\mathbf{r}_R) Y_L(\hat{\mathbf{r}}_R) d\hat{\mathbf{r}}_R, \tag{44}$$

we divide the polyhedron, generated by the well-known Wigner-Seitz approach, into N_t tetrahedra, and we choose a local coordinate system for each tetrahedron. Thus the two dimensional surface integral in (44) may be performed only for the non-equivalent tetrahedra of number N_n, and the total shape function is obtained as

$$\sigma_{RL}(r_R) = \sum_{t}^{N_n} \sum_{i}^{N_e(t)} \sum_{m'} D^l_{m\,m'}(\alpha_i, \beta_i, \gamma_i) \sigma^t_{Rlm'}(r_R), \tag{45}$$

where $D^l_{m\,m'}$ are the matrix elements of finite rotations defined, for example, in Ref. [39], and $\alpha_i, \beta_i, \gamma_i$ are the Euler angles of the local coordinate system associated with the tetrahedron i. In (45) $N_e(t)$ denotes the total number of tetrahedra of type t, i.e. $\sum_t^{N_n} N_e(t) = N_t$.

The angular integration for each non-equivalent tetrahedron was performed by integrating analytically over θ and numerically over ϕ, as described by Stefanou *et al.* [40]. In this way we managed to achieve both high accuracy and efficiency, and thus develop a general algorithm for determining the shape function from the neighboring lattice vectors for an arbitrary structure.

In Fig. 5 we show the $L = (0,0), (4,0), (4,4), (10,0)$ and $(14,0)$ partial components of the shape function for the *bcc* structure as a function of r in units of the lattice constant a. Apart from the spherical component $\sigma_{(0,0)}(r)$, all the other terms are zero inside the inscribed sphere and outside the circumscribed sphere. The partial components of the shape function and their derivatives have kinks at the points where the sphere of radius r passes through a face, an edge or a corner of the polyhedron. In order to ensure the required accuracy in the radial numerical integration we take these points as mesh points.

The partial wave expansion of the shape function (40) oscillates strongly and its convergence towards the step function is rather slow. The insert in Fig. 5 shows the relative error of the volume between the Wigner-Seitz cell and the inscribed sphere, calculated as

$$\begin{aligned} V_{\Omega - S^i} &= \int_{S^c} \sigma(\mathbf{r})\, \sigma(\mathbf{r})\, d\mathbf{r} - \int_{S^i} \sigma(\mathbf{r})\, \sigma(\mathbf{r})\, d\mathbf{r} \\ &= \sum_L \int_{S^i}^{S^c} \sigma_L^2(r)\, r^2\, dr \equiv \sum_l d_l. \end{aligned} \tag{46}$$

As it can be seen from the figure the relative error for $l_{max} = 30$ is still very high (4.2%). However, the partial components exhibit several oscillations within the interval $r \in (S^i, S^c)$ and the number of oscilations increases with the orbital quantum numbers. Therefore, the quantities derived from the shape function by integration like (41) are well behaved, as it can be seen from Fig. 2, where the Hartree energy of *fcc* Cu is shown as a function of l_{max}

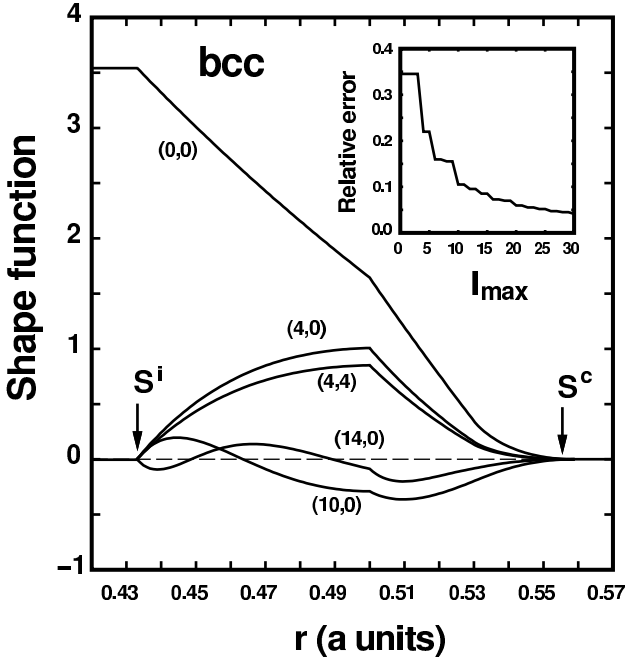

Fig. 5. The partial components of the *bcc* shape function for $L = (0,0),(4,0),(4,4),(10,0)$ and $(14,0)$ as functions of the radius. In the insert the relative error $(V_{\Omega-S^i} - \sum_l^{l_{max}} d_l)/V_{\Omega-S^i}$ (see Eq. (46)) is shown for different l_{max} values.

used in (17) or equivalalently in (43). The figure illustrates that a resonable accuracy is achieved already for $l_{max} = 8 - 12$.

5 Discussion

In this section we review and discuss through several examples some important calculational details related to the FCD total energy calculations. In the self-consistent procedure we solve the scalar-relativistic Dirac equation using either the hamiltonian or the Green's function formalism. In the former description the so called combined correction term [3,5,9] is included. The core electrons are treated within the frozen core approximation, and the semi-core states are included in a second energy panel. In this panel all the l chanels, except that corresponding to the semi-core states, are downfolded [7,8]. In the upper energy panel the inactive chanels are dow-folded. This procedure accounts correctly for the important weak hybrization in the occupied parts of the bandstructure and reduces the rank of the eigenvalue problem to that of the number of active orbitals. Moreover, in this way we manage to avoid the numerical difficulties that arises by fixing the expansion parameter $\epsilon_{\nu\ Rl}$ in a

different position than the center of the occupied part of the corresponding chanel.

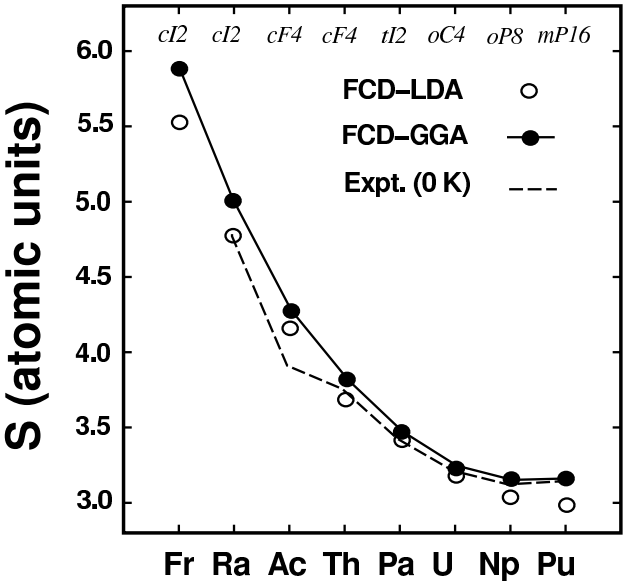

Fig. 6. Equilibrium Wigner-Seitz radii of the light actinides obtained by the full charge density method. The calculations are performed in the LDA or the GGA for the crystallographic α-phases indicated in Pearson notation at the top of the figure. The measured room temperature values are corrected to $T = 0$K using the measured mean thermal expansion coefficients.

As an illustration of this problem we consider the light actinides in the low temperature α phases. The uncorrected ASA fails [37] in the case of these open systems and, therefore, a more accurate and, at the same time, efficient approach is needed. In Fig. 6 we show the equilibrium Wigner-Seitz radii for the light actinides calculated by the present method using either LDA [41,42] or GGA [29] exchange-correlation energy functionals. The crystallographic α phases are indicated in the top of the figure. To obtain fully converged binding energy curves with a proper minimum for the light actinide metals in the FCD method the $6p$ states must be included in the first energy panel and the $7p$ states in a second energy panel. In the first panel we down-folded the s, d and f states and in the second only the p states. For all the active and inactive orbitals the ϵ_ν was fixed at the center of the occupied part of the corresponding band. We have found that the GGA results are on average only 1.3% larger than the zero temperature experimental values. This slight overestimate of the equilibrium volume is a common feature of the GGA functional observed in the case of the transition metals as well [22].

We note that the agrement between the LDA results and the experimental values is very good at the beginning of the series but the experimental trend, reproduced by the GGA, is not properly described by the LDA functional. In order to see the effect of the inactive $7p$ band we fixed $\epsilon_{\nu\,7p}$ at the center of the $7p$ band, thereby reducing the theoretical LDA atomic radius for Th by 2%. Throughout the actinide series the $7p$ band ascends and the errors related to fixing ϵ_ν become smaller. Hence, an incorrect parametrization of the LMTO basis can alter the theoretical trend provided by the FCD method.

The number of orbitals or basis functions that should be considered in the solution of Schrödinger's equation for a crystal potential is one of the basic problems in any band structure calculation method. A low cutoff in the orbital quantum number, i.e., a low l_{max} in (26), prefered in the secular equation, does not always quarantee basis set convergency. Regarding the present method, in several applications we found that the total energy evaluated form the total charge density represents a better basis-set convergence compared to the ASA total energy. In other words, in the case of the transition metals, for example, the inclusion of the f orbitals has a relatively small effect on the FCD total energy, while the ASA total energy can be affected by about 40% [17,18]. This is illustrated in Fig. 7, where we plotted the surface energies of the $4d$ transition metals obtained for the close packed *fcc* (111) surface by means of the LMTO-ASA and FCD methods. The two sets of results correspond to s, p, d and s, p, d, f basis sets. The isotropic experimental values are taken from Ref. [43]. The ASA surface energies and the surface full charge densities, needed for the FCD surface energies, were calculated by means of the self-consistent surface Green's function technique implemented by Skriver and Rosengaard [44]. Details of this calculation can be found in Refs. [17,23]. As it can be seen from the figure, the two sets of FCD results are very close to each other, and in fact they follow the experimental trend. In the ASA calculation the inclusion of the f orbitals has a strong negative effect in the total energy of surface layers. This is due to the fact that in a conventional ASA method the tail expansion (29) is truncated at the same l_{max} as is used for the muffin-tin orbitals. In the FCD technique the truncation in Eq. (29) is always higher than the one in Eq. (26).

The kinetic and exchange-correlation energy functionals used within the FCD technique involve the functional derivatives of the energy densities, see Eq. (9). The first order functional derivative of the exchange-correlation energy, for example, is the well known exchange-correlation potential, μ_{xc}, etc. Some of the parametrized density functionals, however, have different analytical forms for different densities or density gradients, which matches continuously. As a result, they may display an artificial discontinuity in the second or higher derivatives with respect to density or gradient and cannot be applied in conjunction with (9) and (10) which requires simple analytic representations of the exchange-correlation and kinetic energies. Therefore, in the actual applications the exchange-correlation energy is evaluated using

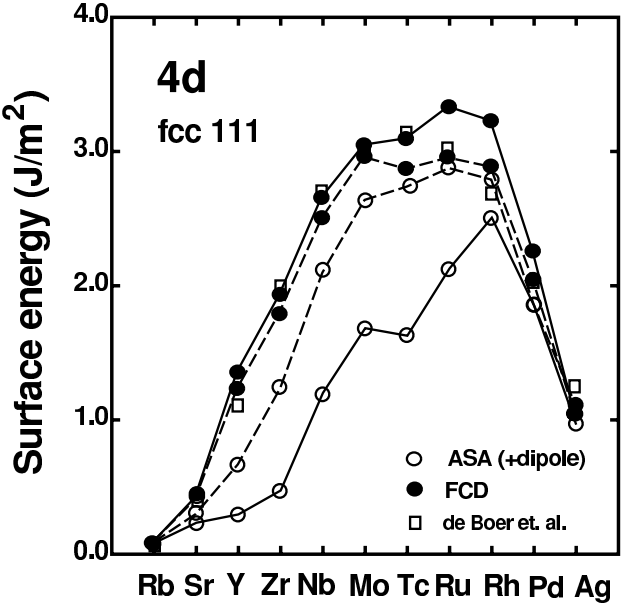

Fig. 7. Comparison of the surface energies obtained using the full charge density LMTO and the LMTO-ASA methods for the *fcc* (111) surface of the 4*d* element. The dashed lines connect the result obtained on the s, p, d basis set, and the solid lines those obtained by inclusion of the f orbitals. The experimental results by de Boer *et al.* are also shown.

either the LDA functional by Perdew and Wang [45], or the GGA functional by Perdew *et. al* [29,46], while the kinetic energy correction, Eqns. (10-13), is evaluated using either the gradient expansion (47) or the Pade's form (52).

In the FCD technique Poisson's equation is solved exactly and, hence, the Coulomb energy is calculated exactly from the total, non-spherical charge density. Moreover, within the LDA or GGA the exchange-correlation energy is also evaluated exactly, and the kinetic energy is corrected for the nonspherical effects. However, the ASA part of the spherical kinetic energy contribution (11) reflects the accuracy of the ASA potential, e.g., how well the spherical part of the full-potential is described by the ASA potential inside the atomic sphere. In open structures with large overlap between the atomic spheres the ASA does not work well and one has to introduce empty spheres into the structure to reduce the overlap and maintain the accuracy of the ASA. As an example of such a system we consider *hexagonal* graphite, where we include 8 empty spheres in the unit cell in addition to the 4 C spheres.

The contour plot of the graphite charge density is shown in Fig. 4. Including 8 empty spheres the true charge density, obtained by the full potential method [36], is equally well reproduced in the C-C direction, in the centre of the hexagonal arrangement of the C atoms and between the atomic layers

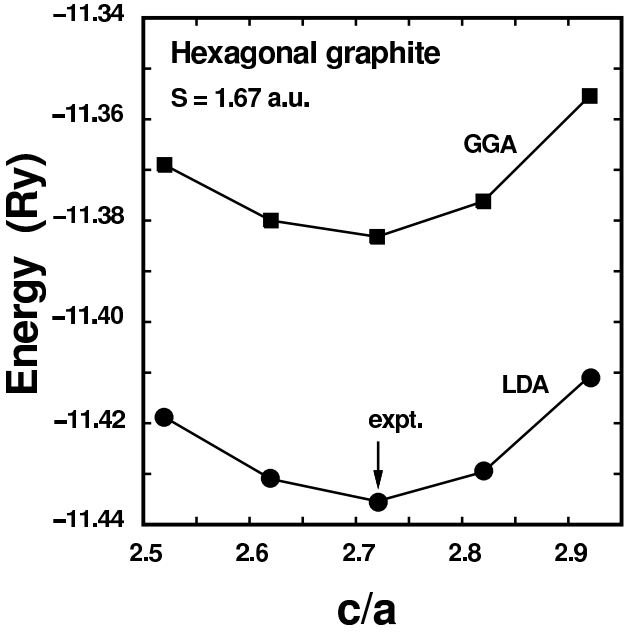

Fig. 8. The total energy of *hexagonal* graphite as a function of the c/a ratio obtained by means of the full charge density LMTO method.

as well. The equilibrium Wigner-Seitz radius and bulk modulus obtained by the present calculation are 1.601 a.u. and 3.32 Mbar within the LDA, and 1.618 a.u. and 3.07 Mbar within the GGA, respectively. These numbers are only in moderate agreement with the experimental values, 1.67 a.u. and 2.86 Mbar [36], and with the full potential results from Ref. [47], 1.68 a.u. and 2.36 Mbar. However, when the c/a ratio is considered, our LDA value shown in Fig. 8 is in very good agreement with both the experimental, 2.72 and full potential value, 2.77 from Ref. [36]. The c/a ratio in the present work was calculated by minimizing the total energy with respect to the c/a at constant volume, like in Ref. [36], and, therefore, it reflects only partially the C-C interlayer bonding.

6 Conclusions

We have presented a full charge density technique based on the complete charge density from a self-consistent LMTO calculation employing a spherically symmetric ASA potential. In the calculations, besides the exact Coulomb and exchange-correlation terms within LDA or GGA, we include a correction to the ASA kinetic energy, which means that we evaluate the true functional rather than an ASA functional. The technique has been tested through several

calculations for systems where the conventional ASA method fails [18,20,22, 23,37]. The comparison with the experimental values and with full potential results shows that the FCD technique has an accuracy similar to that of a full potential description, while the required computational effort is not significantly larger than in conventional spherically symmetric LMTO-ASA calculations.

7 Acknowledgements

This work was supported by the research project OTKA 016740 and 023390 of the Hungarian Scientific Research Fund. The Swedish Natural Science Research Council is acknowledged for financial support. Center for Atomic-scale Materials Physics is sponsored by the Danish National Research Foundation.

8 Appendix A

The starting point for the kinetic energy correction is the density-gradient expansion of the noninteracting kinetic energy functional [28]

$$T[n] = T^{(0)}[n] + T^{(2)}[n] + T^{(4)}[n] + ... \tag{47}$$

with

$$T^{(2k)} = \int t^{(2k)}(\mathbf{r}) d\mathbf{r}. \tag{48}$$

Here, $t^{(2k)}$ is a kinetic energy density which (in atomic Ry units) has the following explicit forms

$$t^{(0)} = \frac{3}{5}(3\pi^2)^{2/3}\, n^{5/3}, \tag{49}$$

$$t^{(2)} = \frac{1}{36}\frac{(\nabla n)^2}{n}, \tag{50}$$

$$t^{(4)} = \frac{1}{370(3\pi^2)^{2/3}}\left[\left(\frac{\nabla^2 n}{n}\right)^2 - \frac{9}{8}\left(\frac{\nabla^2 n}{n}\right)\left(\frac{\nabla n}{n}\right)^2 + \frac{1}{3}\left(\frac{\nabla n}{n}\right)^4\right]. \tag{51}$$

for $k = 0, 1, 2$. This expansion is valid for slowly varying or high densities, i.e. when $s \equiv |\nabla n|/n^{4/3} \ll 1$. For high values of s the expansion diverges

and, therefore, other approximate functional forms should be considered. In the locally truncated expansion suggested in Ref. [48] the number of terms included in the series is determined in each point in space by a local criterion based on the properties of an asymptotic series. In practice, this means that in regions of high gradients the functional reduces to the Thomas-Fermi form, which, obviously, represents a poor approximation to the real kinetic energy density. In Ref. [49] we showed that the local inclusion of the von Weizsäcker term, $t_W = 9t^{(2)}$, rather than the Thomas-Fermi term, gives resonable accurate results in the large gradient limit as well. The parametrized form of this kinetic energy functional is

$$t_{3,2} = t^{(0)} \frac{1 + 0.95x + 9ax^3}{1 - 0.05x + ax^2}, \tag{52}$$

where $x = (5/27)s^2$. The parameter a was determined using the exact Kohn–Sham kinetic energies for the jellium surface [50], and we found $a = 0.396$ [49].

9 Appendix B

To find a reasonable choice for the displacement vector introduced in Eq. (20) we have calculated the electrostatic interaction energy of two truncated spheres of radius S^c with a uniform charge distribution n_0, separated by a distance d [34]. In the case of overlapping bounding spheres, $d < 2S^c$, the intercell energy (20) is given by

$$F^{\text{inter}}[\{Q_l\}] = \sum_l \left(\frac{b_d}{b_d + d}\right)^l \sum_{l',l''} Q_{l'} \times \frac{(l + l' + l'')!}{l!l'!l''!} \frac{1}{(b_d + d)^{l'+l''+1}} Q_{l''}. \tag{53}$$

For nonoverlapping spheres, $d \geq 2S^c$, this expression reduces to the form

$$F^{\text{inter},no}[\{Q_l\}] = \sum_{l,l'} Q_l \frac{(l + l')!}{l!l'!} \frac{1}{d^{l+l'+1}} Q_{l'} \tag{54}$$

where Q_l stands for the l-th multipole moment

$$Q_l = \frac{2\pi n_0}{l+3} (S^c)^{l+3} \int_{-1}^{\frac{d}{2S^c}} P_l(\mathrm{x}) d\mathrm{x} + \frac{2\pi n_0}{l+3} \int_{\frac{d}{2S^c}}^{1} \left(\frac{d}{2x}\right)^{l+3} P_l(\mathrm{x}) d\mathrm{x}. \tag{55}$$

Here $P_l(x)$'s are the Legendre polynomials. We mention that owing to the axial symmetry of the system the multiple moments vanish for $m \neq 0$.

The necessary condition for the convergency of the outer sum in (53) is the convergency of the inner sums over l' and l'' for each value of l. The diagonal terms of the inner sum in (53):

$$A_{l'l'} = {Q_{l'}}^2 \frac{(l+2l')!}{l!(l'!)^2} \frac{1}{(b_d+d)^{2l'+1}} \tag{56}$$

have a maximum around $l' = \tilde{l}$ for $l, l' \gg 1$

$$\tilde{l}(l) = l \frac{\frac{Q_{\tilde{l}+1}}{Q_{\tilde{l}}}}{b_d + d - 2\frac{Q_{\tilde{l}+1}}{Q_{\tilde{l}}}}. \tag{57}$$

From (54) we can estimate the upper limit for the ratio of the multipole moments $\frac{Q_{l+1}}{Q_l}$ since this sum is always convergent for $d \geq 2S^c$ (similar result can be obtained from (55)). Therefore for higher l values we have

$$\frac{Q_{l+1}}{Q_l} < S^c \tag{58}$$

and for $\tilde{l}$ we obtain

$$\tilde{l}(l) < l \frac{S^c}{b_d + d - 2S^c} \equiv \frac{1}{2\alpha} l. \tag{59}$$

Thus we see that the individual terms in the inner sum show a maximum, which (strictly speaking its upper bound) is proportional to l and the coefficient α depends on b_d. In order to ensure the required accuracy of the inner sum it is reasonable to assume that the summation should be carried out at least up to $l'_{max} \simeq \frac{1}{\alpha} l > 2\tilde{l}(l)$ for any l; it is easy to show that in this case for the neglected terms in the inner summmations $\frac{A_{l'l'}}{A_{\tilde{l}\tilde{l}}} < 1\%$. This should hold for the largest value of l as well, i.e. $l_{max} = \alpha l'_{max}$, and we obtain the relation

$$b_d + d = (1+\alpha)\, 2S^c. \tag{60}$$

The validity of this choise of the displacement vector should hold for realistic systems as well because in (58) for the ratio of the multipole moments we use an estimate which is independent on the shape of the cell and on the charge distribution. We note that Eq. (24) is a generalization of (60).

On the basis of (60) we can explain the existence of the range of convergence in the outer summation. For a fixed value of l'_{max} it is obvious that with increasing l, we start to neglect significant terms in the inner summation if $\frac{1}{\alpha}l > l'_{max}$ which may lead to the divergence of the outer sum. Therefore an upper limit of the range of convergence in l may be defined as $l'_{max}\left(\frac{b_d+d}{2S^c}-1\right)$. Thus with increasing b_d the range of convergence becomes wider in accordance with the observation by Gonis *et al.* ([33]).

10 Appendix C

In the linear muffin-tin orbitals method [1,2,3,4,5,6,7,8,9] the lower part of the tail functions are substituted (taking into account the normalization function) by the first energy derivative of the partial wave, $\dot{\varphi}^\gamma$ calculated at the center of the energy range of interest, ϵ_ν. In this way the LMTO's become energy independent up to the second order and the summation over the occupied states in (38) can be evaluated separately. The energy dependence of the envelope functions within the LMTO formalism is fixed at $\kappa^2 = 0$. In the following we use the nearly orthogonal representation (γ) but the relations can easily be generalized to other representations.

The second order expression for the wave function (34) that includes the high tail contributions becomes

$$\begin{aligned}\psi(\epsilon_j, \mathbf{r}_{R'}) = &\sum_{L'}[\varphi_{R'L'}(\mathbf{r}_{R'}) + \frac{1}{2}(\epsilon_j - \epsilon_{\nu\, R'l'})^2\ddot{\varphi}_{R'L'}(\mathbf{r}_{R'})]u^j_{R'L'} \\ &+ \sum_{L'}\tilde{j}^\gamma_{R'L'}(\mathbf{r}_{R'})\tilde{u}^j_{R'L'},\end{aligned} \tag{61}$$

where $\ddot{\varphi}$ denotes the second order energy derivative. The first summation includes terms up to the $l_{max} \leq 2$(or 3), while the second summation includes all the high l' tail components as well. In (61) we have introduced a compact notation for the tail functions

$$\tilde{j}^\gamma_{R'l'}(r_{R'}) = \begin{cases} \dot{\varphi}^\gamma_{R'l'}(r_{R'}) & \text{if } l' \leq l_{max}, \\ j_{l'}(r_{R'}) & \text{if } l' > l_{max} \end{cases}, \tag{62}$$

and for the eigenvectors

$$\tilde{u}^j_{R'L'} = \begin{cases} (\epsilon_j - \epsilon_{\nu\, R'l'})u^j_{R'L'} & \text{if } l' \leq l_{max}, \\ -\sum_{RL} S^\gamma_{R'L',RL}\frac{1}{\sqrt{\frac{S}{2}\dot{P}^\gamma_{Rl}}}u^j_{RL} & \text{if } l' > l_{max} \end{cases} \tag{63}$$

In (61) the partial waves, their energy derivatives and the energy derivative of the potential function are calculated at $\epsilon = \epsilon_\nu$. Now we can write the expression for the partial components of the full charge density,

$$n_{RL} = \sum_{L''L'} C^{L}_{L''L'}[\varphi_{Rl''}\varphi_{Rl'}m^{0}_{RL''L'} + \varphi_{Rl''}\tilde{j}^{\gamma}_{Rl'}m^{1}_{RL''L'} + \frac{1}{2}\varphi_{Rl''}\ddot{\varphi}_{Rl'}m^{2}_{RL''L'} + +\tilde{j}^{\gamma}_{Rl''}\varphi_{Rl'}(m^{1}_{RL'L''})^{*} + \frac{1}{2}\ddot{\varphi}_{Rl''}\varphi_{Rl'}(m^{2}_{RL'L''})^{*} + \tilde{j}^{\gamma}_{Rl''}\tilde{j}^{\gamma}_{Rl'}m^{3}_{RL''L'}], \quad (64)$$

where for simplicity we have neglected the radial variable r_R, and

$$m^{0}_{RL''L'} = \sum_{j}^{occ.} u^{j\,*}_{RL''}u^{j}_{RL'} \qquad \text{if } l'', l' \le l_{max},$$

$$m^{1}_{RL''L'} = \sum_{j}^{occ.} u^{j^{*}}_{RL''}\tilde{u}^{j}_{RL'} \qquad \text{if } l'' \le l_{max},$$

$$m^{2}_{RL''L'} = \sum_{j}^{occ.} u^{j\,*}_{RL''}(\epsilon_j - \epsilon_{\nu\,Rl'})^2 u^{j}_{RL'} \quad \text{if } l'', l' \le l_{max},$$

$$m^{3}_{RL''L'} = \sum_{j}^{occ.} \tilde{u}^{j^{*}}_{RL''}\tilde{u}^{j}_{RL'} \qquad .$$

In (64) the l'' and l' summations include the high tail components as well, however, for these high indices the φ and $\ddot{\varphi}$ should be set to zero.

The high-low block of the structure constant S^{γ} can be calculated using the Dyson equation

$$S^{\gamma}_{R'L',RL} = S^{\alpha}_{R'L',RL} + \sum_{R''L''} S^{\alpha}_{R'L',R''L''}(\gamma_{R''l''} - \alpha_{R''l''})S^{\gamma}_{R''L'',RL}, \quad (65)$$

where $\gamma_{R''l''} = \alpha_{R''l''} = 0$ for $l'' > l_{max}$, and the high-low subblock of the tight-binding LMTO structure constant S^{α} is obtained from (36) written for $\kappa^2 = 0$.

References

1. O.K. Andersen, Solid State Commun. **13**, 133 (1973).
2. O.K. Andersen and R.G. Wolley, Mol. Phys. **26**, 905 (1973).
3. O. K. Andersen, Phys. Rev. B **12**, 3060 (1975).
4. A.R. William, J. Kübler, and C.D. Gelatt, Phys. Rev. B **19**, 6094 (1979).
5. H.L. Skriver, *The LMTO Method* (Springer-Verlag, Berlin, 1984).
6. O.K. Andersen and O. Jepsen, Phys. Rev. Lett. **53**, 2571 (1984).
7. O.K. Andersen, O. Jepsen, and D. Glötzel, in *Highlights of Condensed-Matter Theory* , edited by F. Bassani, F. Fumi, and M. P. Tosi (North Holland, New York, 1985).

8. W.R.L Lambrecht and O.K. Andersen, Phys. Rev. B **34**, 2439 (1986).
9. O.K. Andersen, Z. Pawlowska, and O. Jepsen, Phys. Rev. B **34**, 5253 (1986).
10. G.W. Fernando, B.R. Cooper, M.V. Ramana, H. Krakauer, and C.Q. Ma, Phys. Rev. Lett. **56**, 2299 (1986).
11. J.M. Wills and B.R. Cooper, Phys. Rev. B **36**, 3809 (1987).
12. M. Springborg and O.K. Andersen, J. Chem. Phys. **87**, 7125 (1987).
13. M. Methfessel, Phys. Rev. B **38**, 1537 (1988).
14. M. Methfessel, C.O. Rodriguez, and O.K. Andersen, Phys. Rev. B **40**, 2009 (1989).
15. S. Savrasov and D. Savrasov, Phys. Rev. B **46**, 12181 (1992).
16. P. Hohenberg and W. Kohn, Phys. Rev. **136B** 864 (1964).
17. L. Vitos, J. Kollár and H. L. Skriver, Phys. Rev. B **49**, 16694 (1994).
18. J. Kollár,L. Vitos, and H. L. Skriver, Phys. Rev. B **49**, 11288 (1994).
19. J. Kollár, L. Vitos and H. L. Skriver, NATO ASI Series, Vol.41, ed. P. A. Sterne, A. Gonis and A. A. Borovoi, p.97 (1998)
20. L. Vitos, J. Kollár, and H. L. Skriver, Phys. Rev. B **55**, 4947 (1997).
21. J. Kollár, L. Vitos and H. L. Skriver, Phys. Rev. B **55**, 15353 (1997).
22. L. Vitos, J. Kollár, and H. L. Skriver, Phys. Rev. B **55**, 13521 (1997).
23. L. Vitos, A.V. Ruban, H. L. Skriver and J. Kollár, Surface Sci. **411**, 186 (1998)
24. L. Vitos, A.V. Ruban, H. L. Skriver and J. Kollár, Phil. Mag. **78**, 487 (1998)
25. O.K. Andersen, O. Jepsen, and G. Krier, in *Methods of Electronic Structure Calculations* , edited by V. Kumar, O.K. Andersen, and A. Mookerjee (World Scientific, Singapore, 1994), p. 63.
26. W. Kohn and L.J. Sham, Phys. Rev. **140** A1133 (1965).
27. A.E. DePristo and J.D. Kress, Phys. Rev. A **35**, 438 (1987).
28. R.M. Dreizler and E.K.U. Gross, Density Functional Theory, (Springer-Verlag, 1990).
29. J. D. Perdew, in *Electronic Structure of Solids*, edited by P. Ziesche and H. Eschrig, Academic Verlag, Berlin, p. 11 (1991).
30. O.K. Andersen, O. Jepsen and M. Sob, in Electronic Band Structure and its Applications, ed. M. Yussouff (Springer Lecture Notes, 1987).
31. P. Söderlind, O. Eriksson, J.M. Wills and A.M. Boring, Phys. Rev. B **48**, 5844, (1993)
32. J. van W. Morgan, J. Phys. C, **10**, 1181 (1977)
33. A. Gonis, E. C. Sowa and P. A. Sterne, Phys. Rev. Lett. **66**, 2207 (1991)
34. L. Vitos and J. Kollár, Phys. Rev. B **51**, 4074, (1995).
35. O.K. Andersen, A.V. Postnikov and S.Yu. Savrasov, in Applications of Multiple Scattering Theory to Materials Science, Eds. W.H. Butler, P.H. Dederichs, A. Gonis and R.L. Weaver, MRS Symp. Proc. p.37 (1992)
36. R. Ahuja, S. Auluck, T. Trygg, J. M. Wills, O. Eriksson, and B. Johansson, Phys. Rev. B **51**, 4813 (1995).
37. L. Vitos, J. Kollár, and H. L. Skriver in NATO ASI Series B:Physics, Stability of Materials, ed. A. Gonis, P.E.A. Turchi and J. Kudrnovsky, p. 393, Plenum Press, New York (1996).
38. B. Drittler, M. Weinert, R. Zeller and P. H. Dederichs, Solid State Commun. **79**, 31, (1991)
39. A.R. Edmonds, Angular Momentum in Quantum Mechanics, Ed. by E. Wigner and R. Hofstadter, Princeton University Press, Princeton, (1957)
40. N. Stefanou, H. Akai and R. Zeller, Comput. Phys. Comun. **60**,231 (1990)

41. J. Perdew and A. Zunger, Phys. Rev. B **23**, 5048 (1981).
42. D. M. Ceperley and B. J. Alder, Phys. Rev. Lett. **45**, 566 (1980).
43. F. R. de Boer, R. Boom, W. C. M. Mattens, A. R. Miedema, and A. K. Niessen, *Cohesion in Metals* (North-Holland, Amsterdam, 1988).
44. H.L. Skriver and N. M. Rosengaard, Phys. Rev. B **46**, 7157 (1992).
45. J. Perdew and Y. Wang, Phys. Rev. B **45**, 13244 (1992).
46. J.P. Perdew, K. Burke, and M. Ernzerhof, Phys. Rev. Lett. **77**, 3865 (1996).
47. M. T. Yin, Marvin. L. Cohen, Phys. Rev. B **29**, 6996 (1984).
48. E.W. Pearson, and R.G. Gordon, J. Chem. Phys. **82**, 881 (1985)
49. L. Vitos, H. L. Skriver, and J. Kollár, Phys. Rev. B **57**, 12611 (1998).
50. N. D. Lang and W. Kohn, Phys. Rev. B **1**, 4555 (1970).